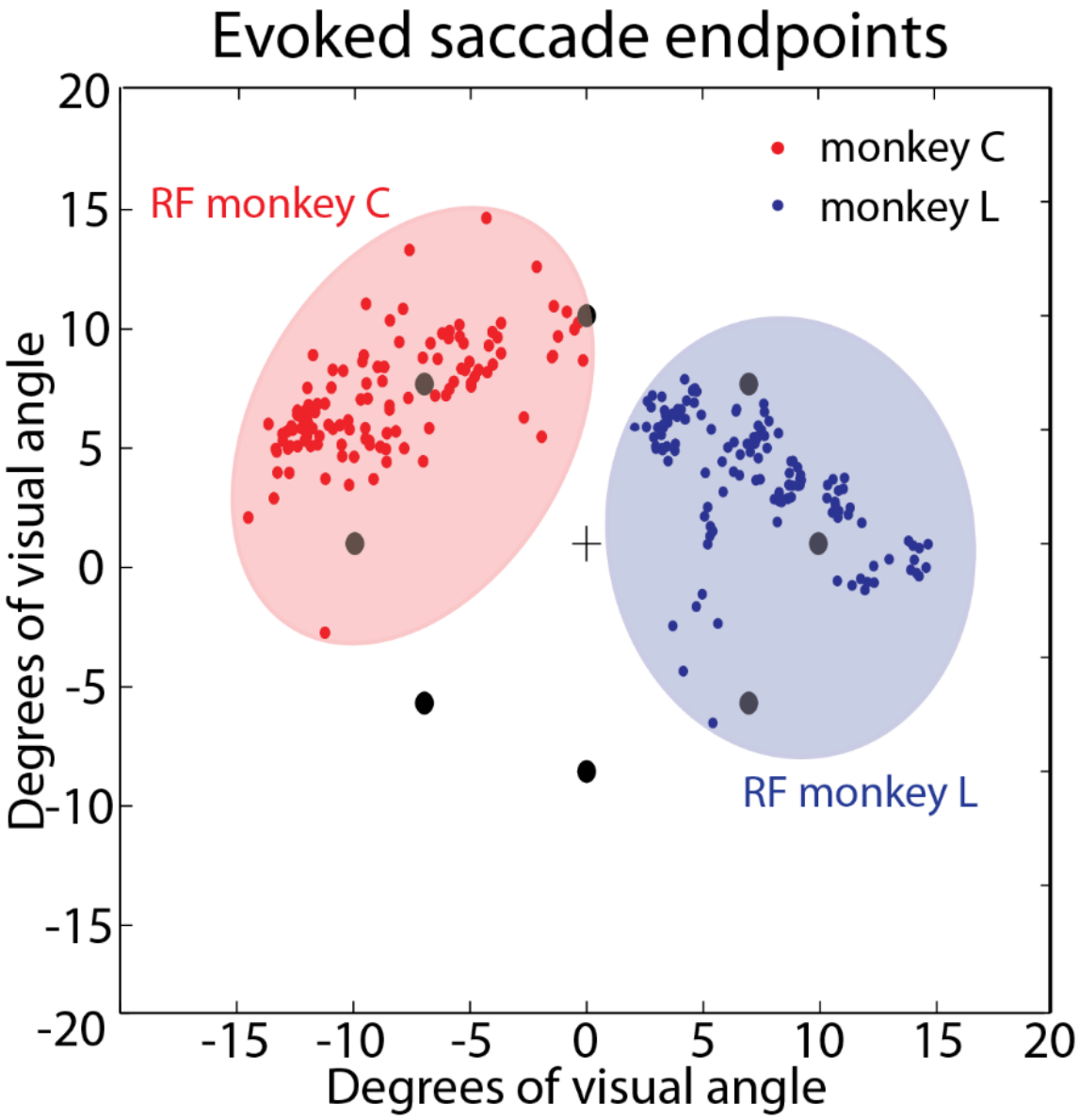

Supplementary Figure 1. Receptive fields evoked in both monkeys

End points of saccades evoked using micro-stimulation in the injection sites in both monkeys with 0.25mm depth spacing (see Online Methods). All end points are relative to a saccade that started in the central fixation location (0, 0) denoted with the cross. The possible target locations, each with an eccentricity of 10° are shown as black circles. The general receptive fields (RFs) for both monkeys are circled and shaded in red (Monkey C) or blue (Monkey L).

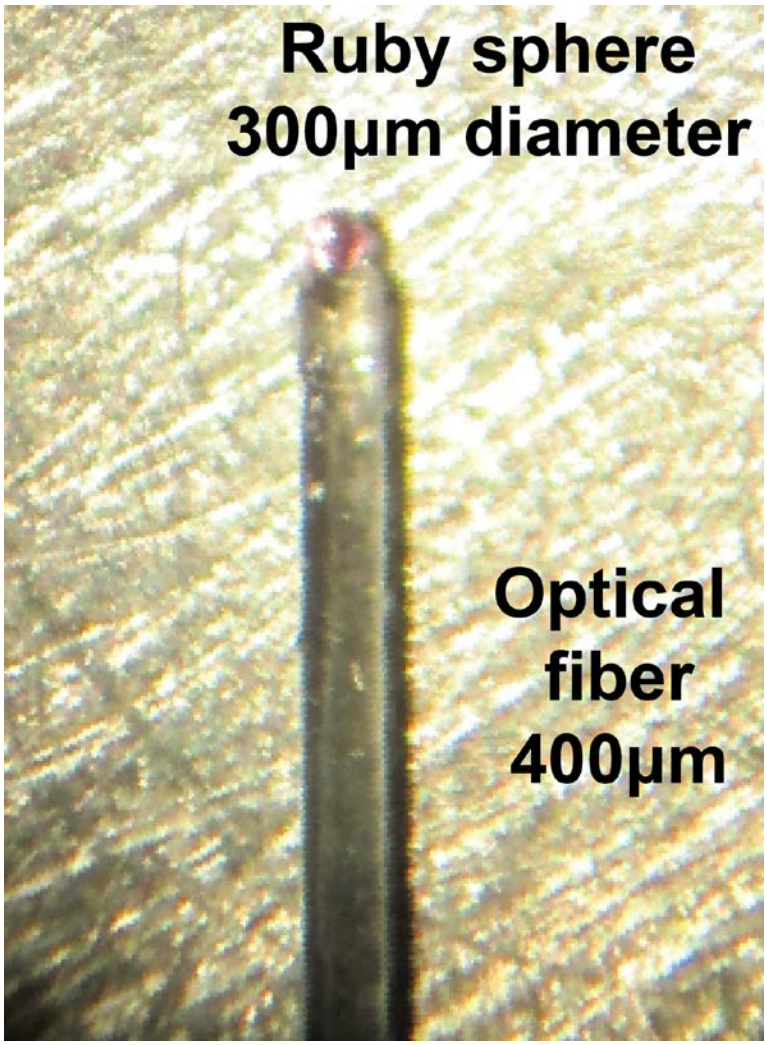

Supplementary Figure 2. Isometric ruby-tipped light probe
Isometric, ruby-tipped light probes were constructed by affixing a 300 µm diameter spherical ruby ball lens (NT46-223, Edmund Optics) to the flat-cleaved, polished end of a 400 µm diameter multimode optical fiber (ThorLabs, BFH48-400, NA = 0.48) with optically-transparent, UV curable adhesive (NT37-322, Edmund Optics). When photons of applied light struck this probe, the ruby tip emitted photons in a random direction independent of the incident photon direction. Measurement of these emitted photons allows for isometric light power measurements.

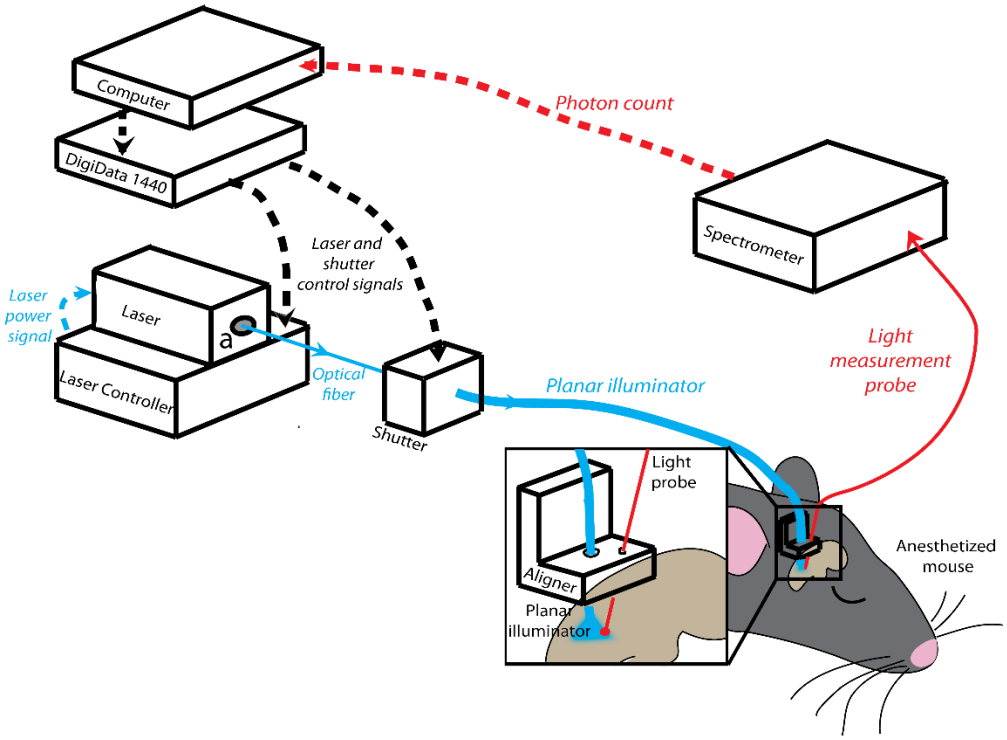

Supplementary Figure 3. A strategy for *in vivo* measurement of visible light propagation.
a) Set up for *in vivo* light measurements with isometric light probe. **b)** Average light decrease with distance from the illuminator: Mean normalized fluence rates representing the fraction of applied light power reaching a given depth for blue (473 nm), green (532 nm) and red (635 nm) light as a function of distance from the illuminator with standard error bars. (n = 5 mice for 473 nm; n = 6 mice for 532 nm; and n = 5 mice for 635 nm).

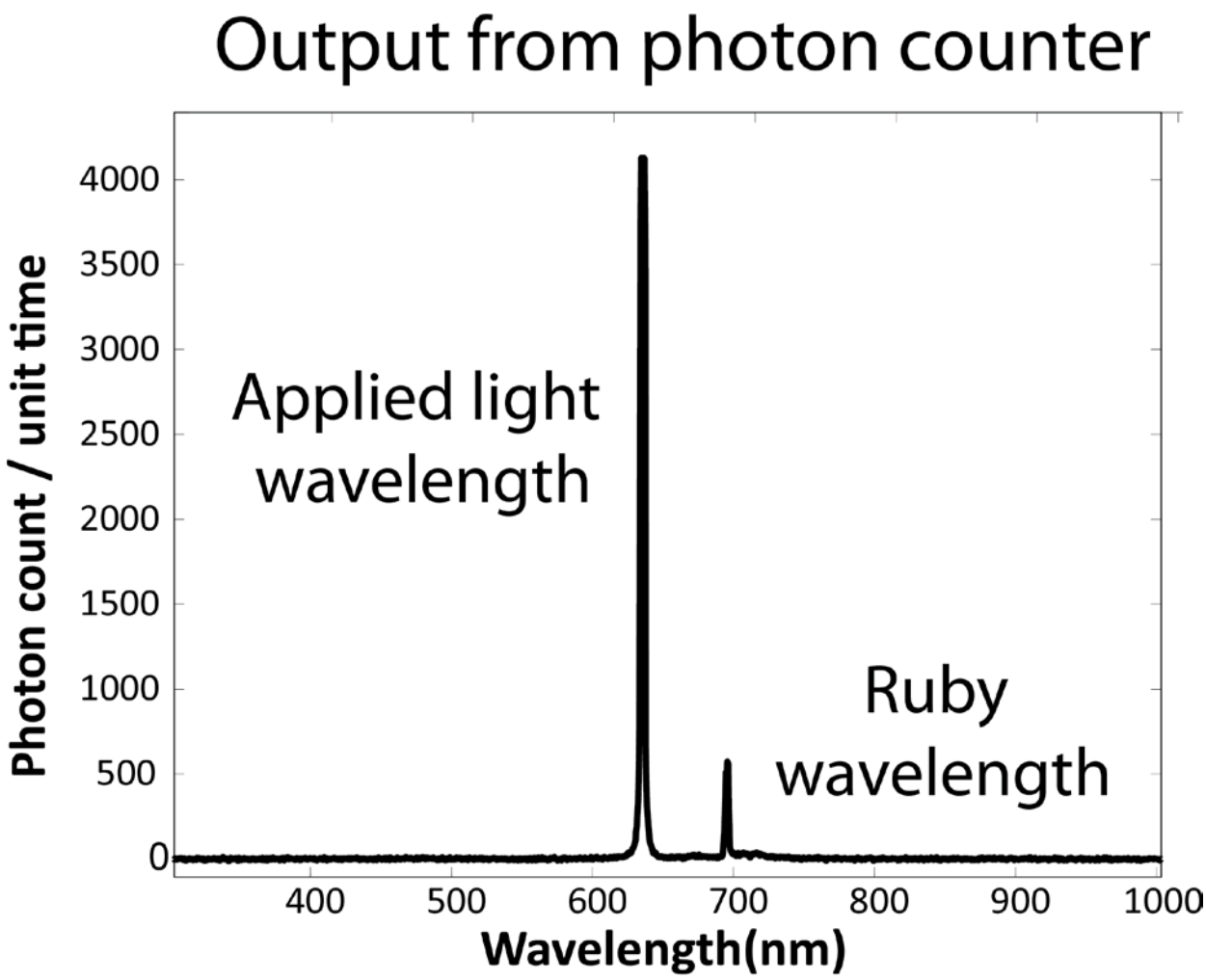

Supplementary Figure 4. Photon count from an isometric ruby-tipped light probe output
Sample spectrometer measurement of the photon count from an isometric ruby tipped light probe shows two peaks. The first peak (635 nm) is an artifact from applied light that struck the probe somewhere other than the tip. The second peak, which is used for light power measurements, reflects the ruby fluorescence induced by the incident light at the tip.

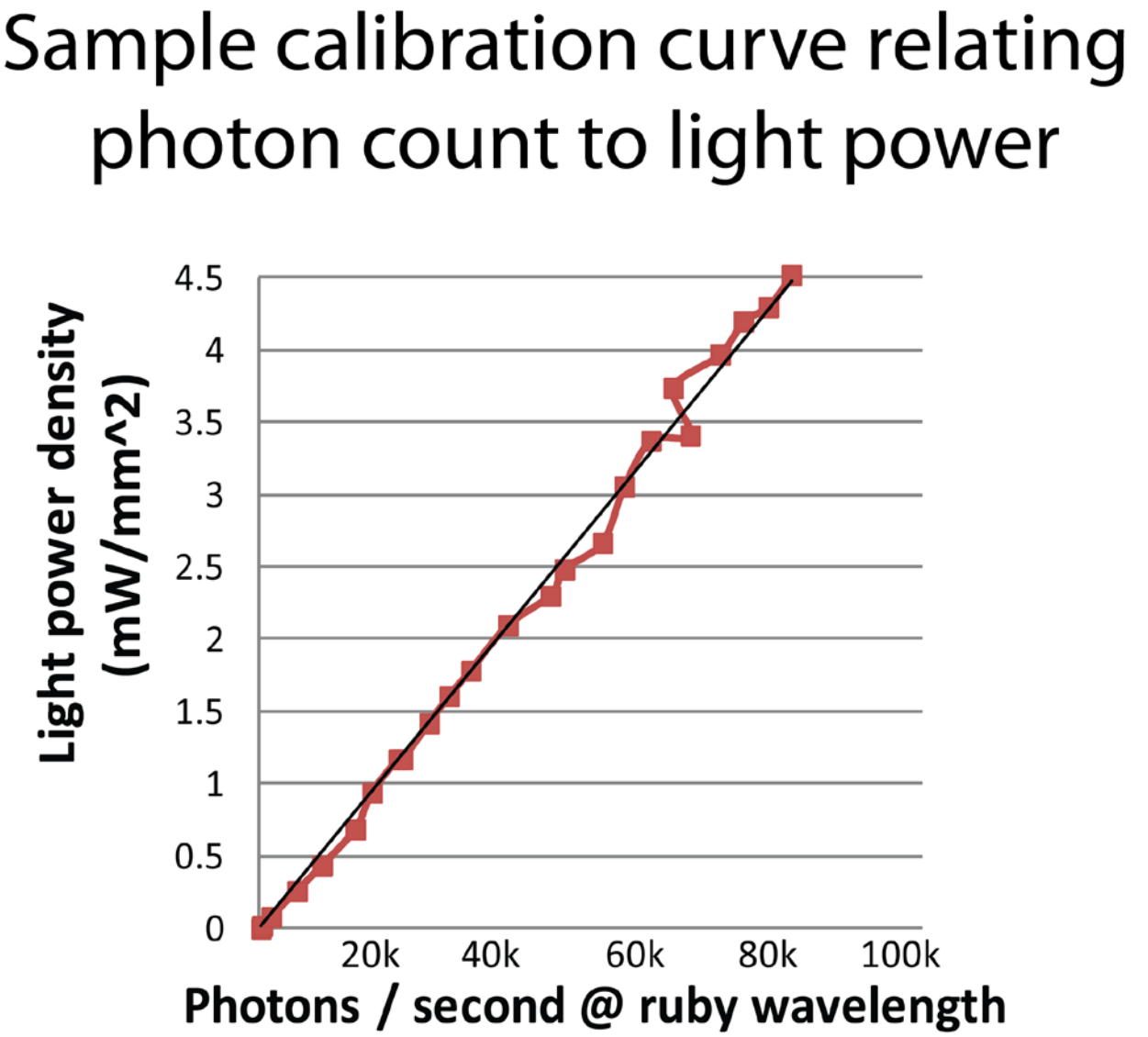

Supplementary Figure 5. Isometric ruby-tipped light probe calibration
An example calibration curve for a isometric ruby-tipped light probe is shown. Light power densities of 0.25 to 4.5 mW /mm^2 were applied to each probe in 0.25 mW /mm^2 increments. The rate of ruby photon emission was measured for each of these applied light power densities and light power density was plotted as a linear function of the ruby photon emission rate. The slope of the calibration curve was then used to relate photon counts measured in vivo to the incident light power density. The intercept for the curve was fixed at 0 because the spectrometer was "dark-corrected" prior to each recording session such that no incident light yielded a photon count of 0.

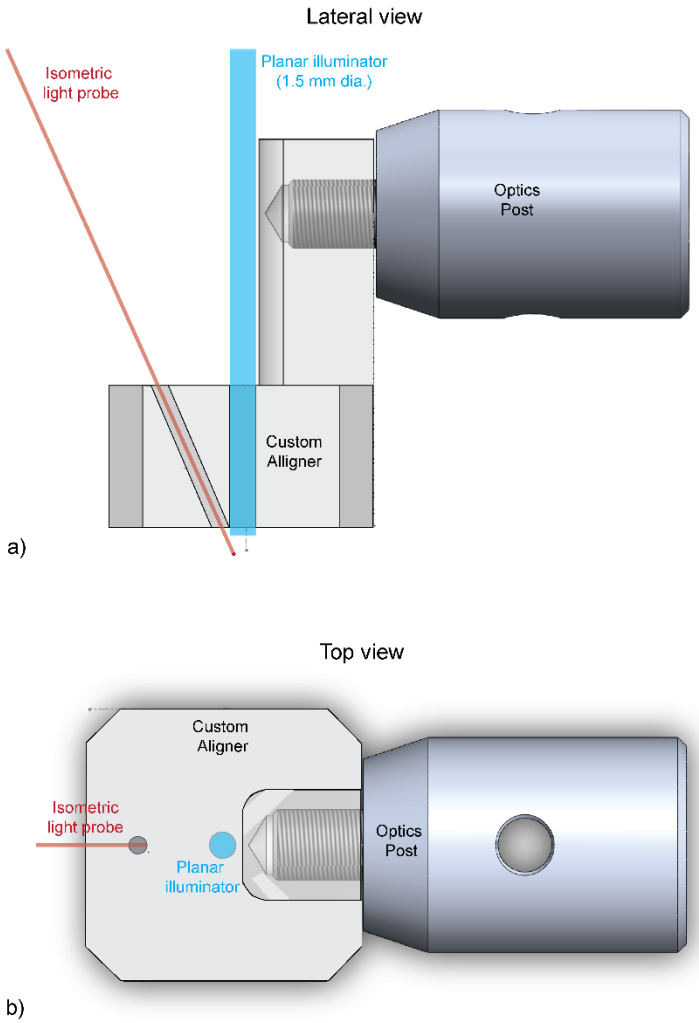

Supplementary Figure 6. Custom aligner for *in vivo* light measurements
(A) The large diameter optic fiber (labeled as “planar illuminator”) was affixed in the center of a 3D printed custom aligner. The isometric ruby-tipped light probe was lowed through a trajectory formed in the custom aligner at a 28 degree angle. This custom aligner interfaced with an optical post (ThorLabs) and was stereotactically lowered on to the surface of the mouse brain. (B) The custom aligner is shown from the side. Additional holes were present, but not used.

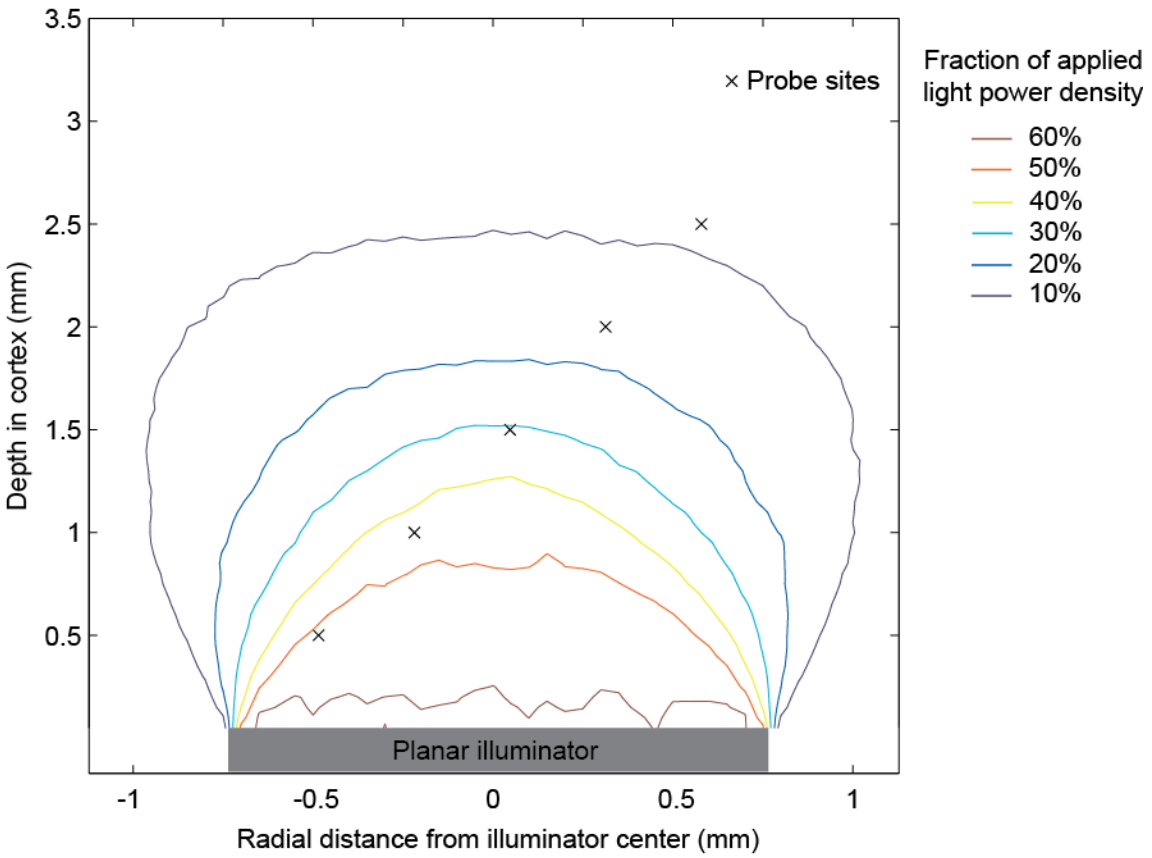

Supplementary Figure 7: Monte Carlo Model of the planar illuminator

Monte Carlo model demonstrates that the planar illuminator light distribution is even over the areas that we illuminate with respect to the illuminator axis. Thus, at each depth, our probe sees the same intensity that it would if it were directly under the center of the illuminator

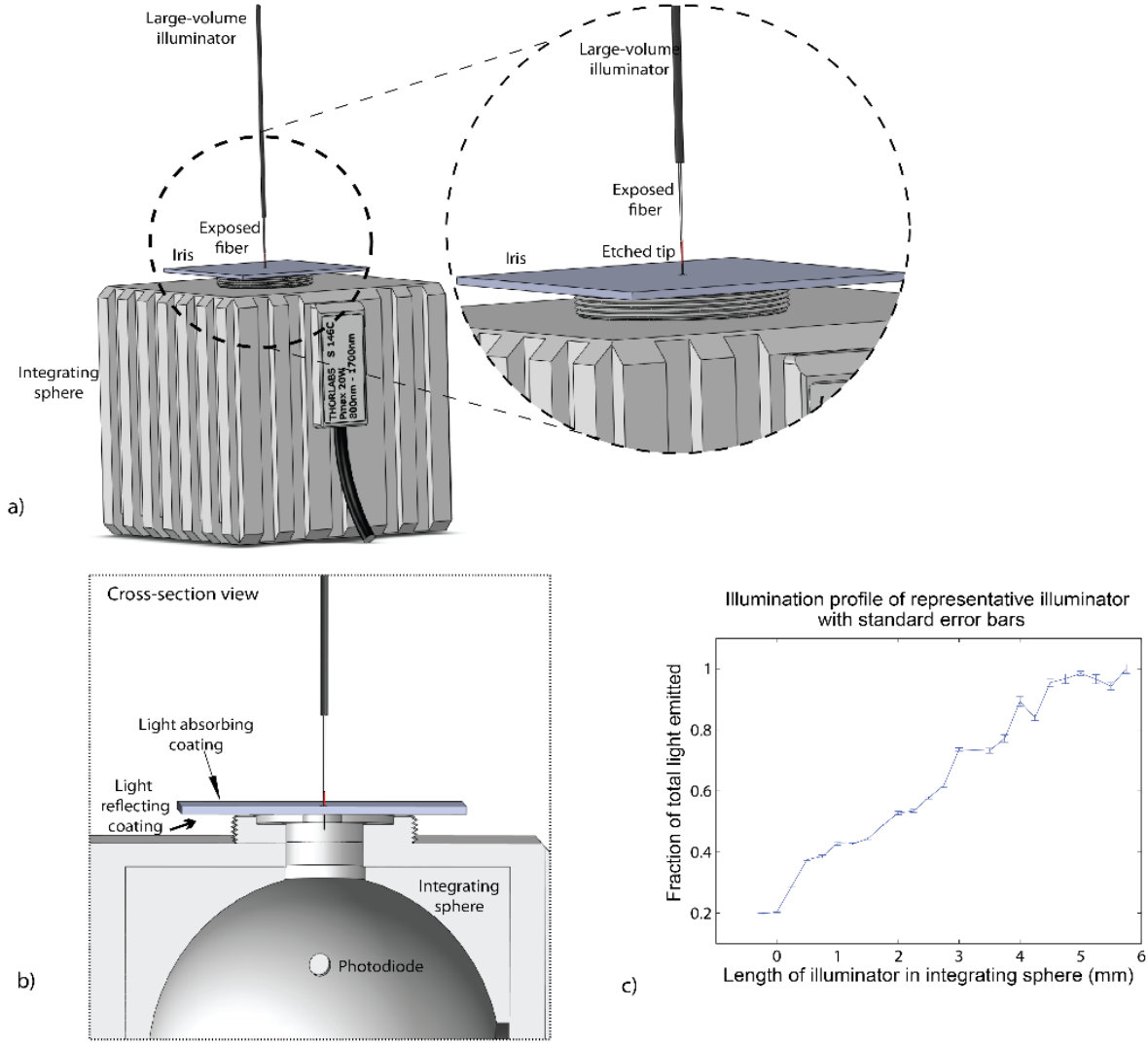

Supplementary Figure 8. Large-volume illuminator calibration

(A) External view of large volume illuminator as it is lower into an integrating sphere covered with a custom iris, such that light emitted above the iris is absorbed and light emitted below the iris is reflected into the sphere for measurement. (B) Cross-sectional view of illuminator profiling set up. (C) Representative illuminator profile with the fraction of total light emission measured as a function of the length of the illuminator that is in the integrating sphere to be measured. An even light emitting surface is critical for the prevention of "hot spots." Specifically, only a small amount (<25%) of total light is emitted at the tip. This calibration ensured that each large volume illuminator distributed light evenly over a large volume.

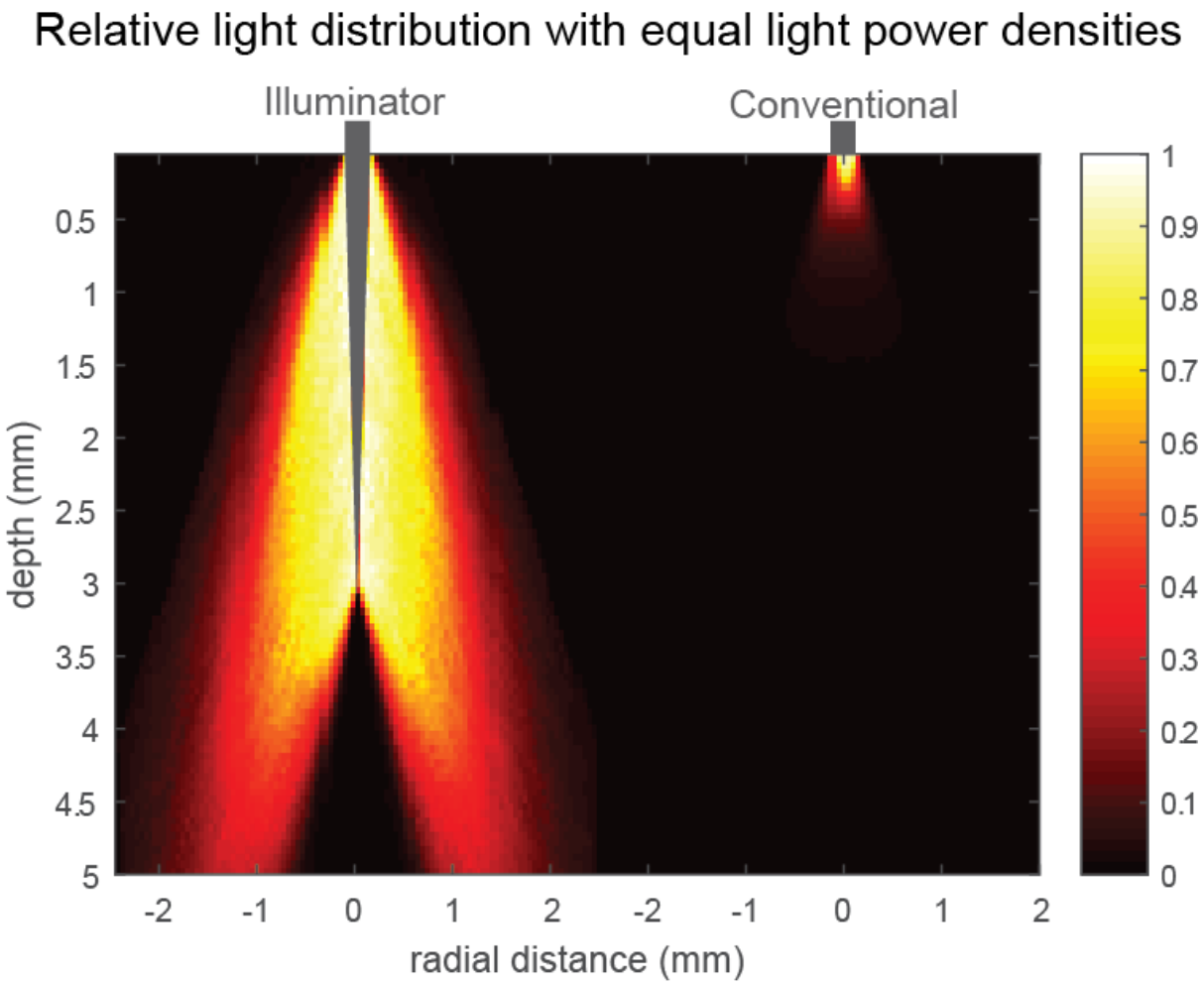

Supplementary Figure 9: Monte Carlo model
Side-by-side Monte Carlo models of a middle cross section of the illuminator (with 3 mm tip length) and a conventional flat-cleaved optical fiber withequal light power densities on their respective surfaces. These 2D models show what the recorded neurons lateral to, and below, the illuminator would see. The 3D profile shapes observed in the brain phantom in **Fig. 3** would result from rotation of these profiles along the axis of the illuminator to yield a 3D representation.

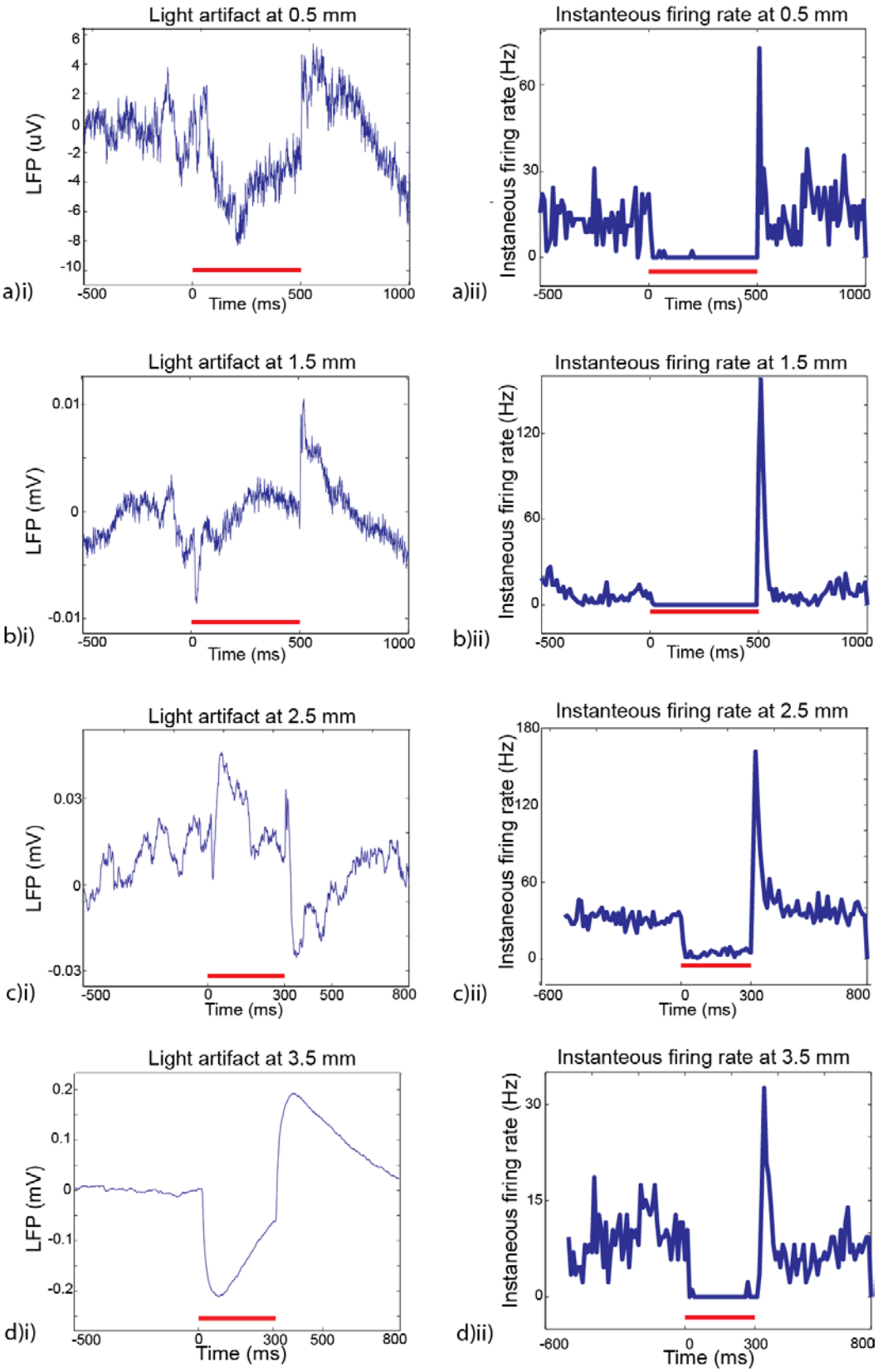
Light artifact at 0.5 mm
LFP (uV)
Time (ms)
a)i)
Instanteous firing rate at 0.5 mm
Instaneous firing rate (Hz)
Time (ms)
a)ii)
Light artifact at 1.5 mm
LFP (mV)
Time (ms)
b)i)
Instanteous firing rate at 1.5 mm
Instaneous firing rate (Hz)
Time (ms)
b)ii)
Light artifact at 2.5 mm
LFP (mV)
Time (ms)
c)i)
Instanteous firing rate at 2.5 mm
Instaneous firing rate (Hz)
Time (ms)
c)ii)
Light artifact at 3.5 mm
LFP (mV)
Time (ms)
d)i)
Instanteous firing rate at 3.5 mm
Instaneous firing rate (Hz)
Time (ms)
d)ii)

S. Fig. 10

Supplementary Figure 10. LFP changes with illumination in monkey C

Local field potential recordings of representative neurons along the injection trajectory of monkey C (left column) and instantaneous spike time histograms at the same locations (right column). The red bar denotes when the laser is on. Note that the virus injections were performed at depths of 0.6 mm relative to the surface of cortex to 3.5 mm relative to the surface of cortex in 0.6 mm intervals. All of this data comes from single contact recordings in Subject C. The shape of the light artifact shown here differs from what was observed Fig. 2g, likely due, at least in part, to electrode differences: u-probe in **Fig. 2g** and a single contact parylene-coated tungsten microelectrode here.

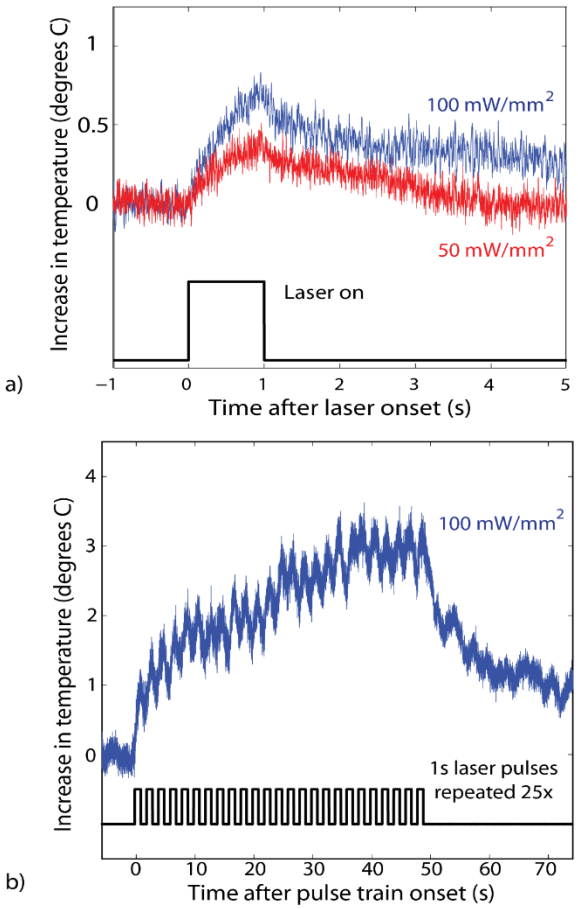

Supplementary Figure 11*. In vivo* temperature measurements with large-volume illuminator
a) Real-time temperature measurements for 1 second 50 mW/mm^2 and 100 mW/mm^2 red (635 nm) light pulses delivered via a large volume illuminator in mouse cortex. Four probes were placed along the illuminator and the probe with the maximum increase relative to baseline is shown. **b)** The heat relaxation time of brain tissue was measured as a train of 1s pulses was applied in the same preparation described above. By fitting the relaxation traces for the curves, we determined that we needed to wait 20 times the pulse duration to prevent any additive heating. In the actual testing, the average time from the start of one trial to the start of the next was about 2 s. With a laser pulse duration of 0.3 s, we determined that we should illuminate no more frequently than once every third trial to avoid heating and weighted the non-laser and laser conditions accordingly.

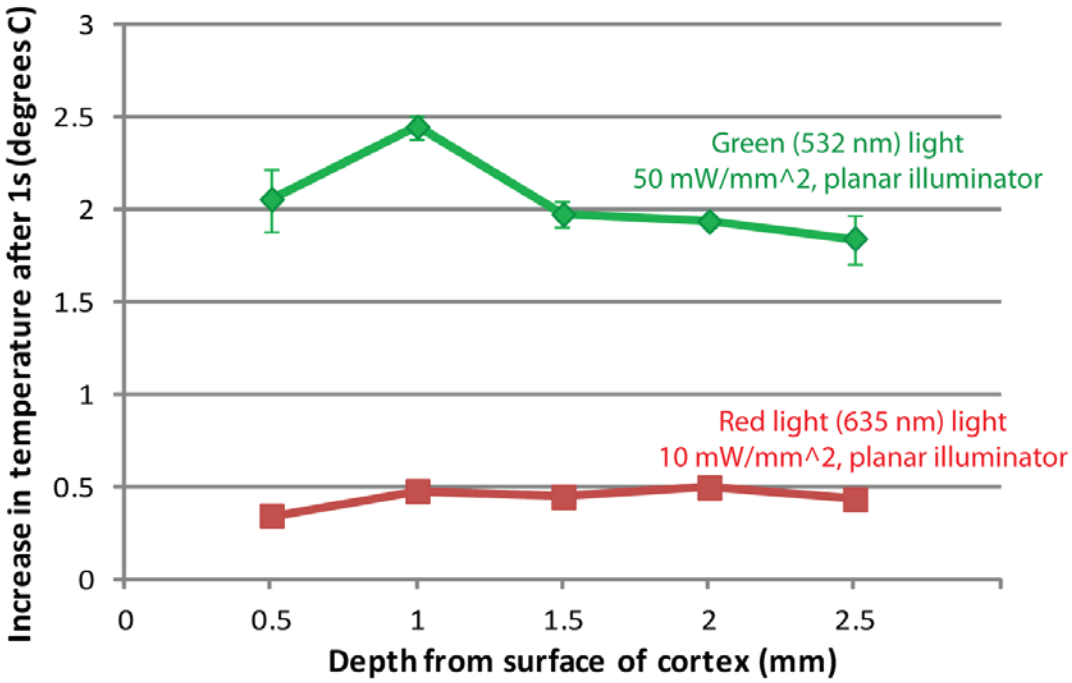

Supplementary Figure 12: Heat measurements at various distances from light source.
In vivo measurements of tissue heating with a large diameter planar illuminator showing that the temperature increase peaks at 1 mm from the light source. **N = 5 mice for each trace.**

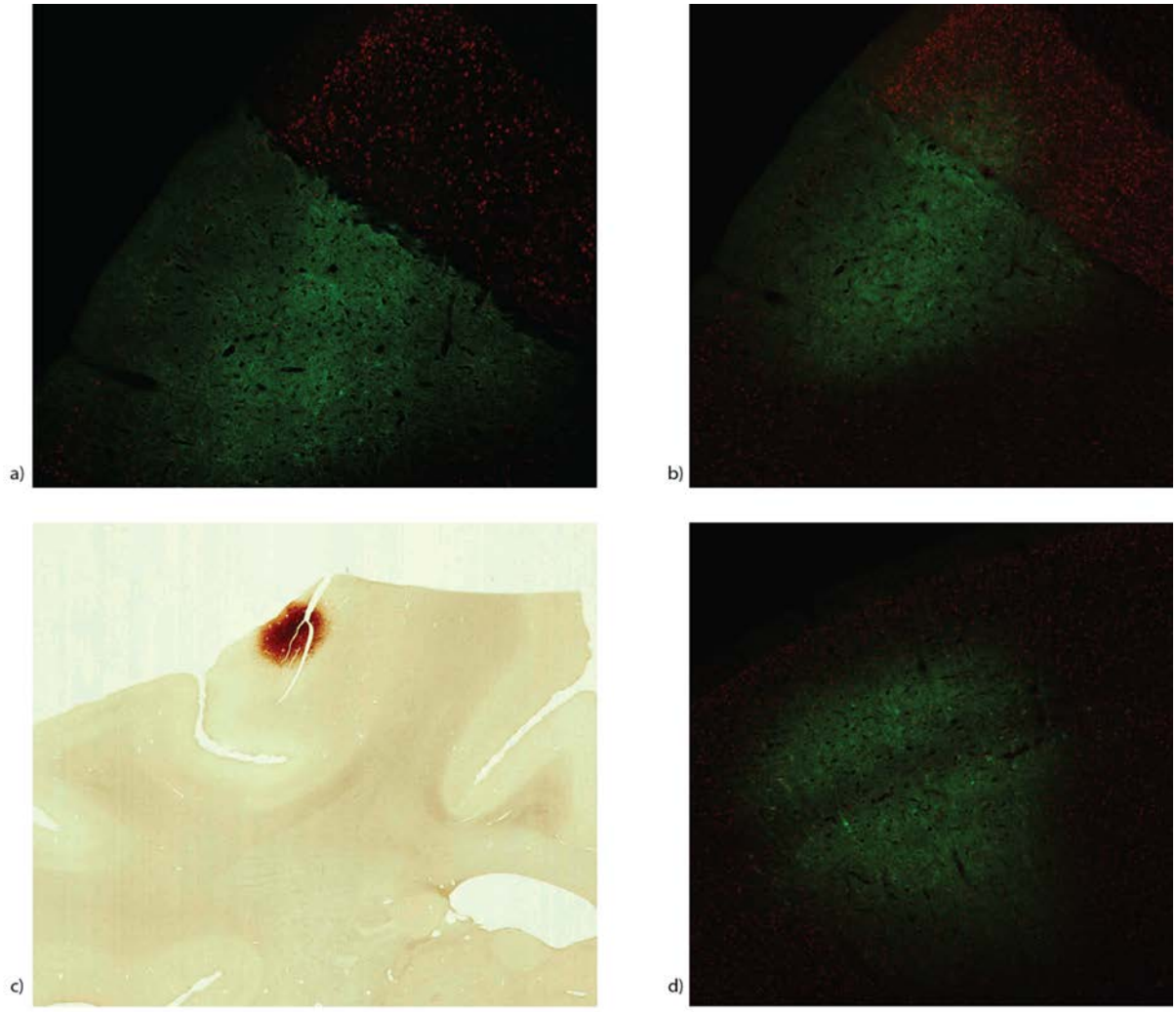

Supplementary Figure 13. AAV8-hSyn-Jaws-GFP expression in macaque FEF

a) AAV8-hSyn-Jaws_GFP expression in macaque FEF. 2 µm thick confocal image of macaque FEF (Monkey R) that was injected with 0.8 µL of AAV8-hSyn-Jaws-GFP diluted to a titer of 6 x 10^{11} particles / mL. at each of four sites spaced 0.6 mm apart in FEF using the techniques described in the methods. The image shows the injected area clearly (including needle tract on the far left side of the image) and tissue in which there was no expression. The similar cell densities in both tissues imply that viral expression did not impact cell health. Neurons are stained in red with NeuN while GFP expression is show in green. In the injected gyrus, 1523/1660 neurons (91.7%) stained green as well, indicating GFP co-expression and viral infection. The sharp line delineating the two regions is the result of a post-perfusion crack in the tissue, illustrated in a DAB stained section from the same region b). b) DAB stained section from the same region imaged with a light microscope. c) Composite image of the entire 50 µm thick section encompassing a). d) section from a site about 1 mm distal to the center of the injection site is shown in a)-c)

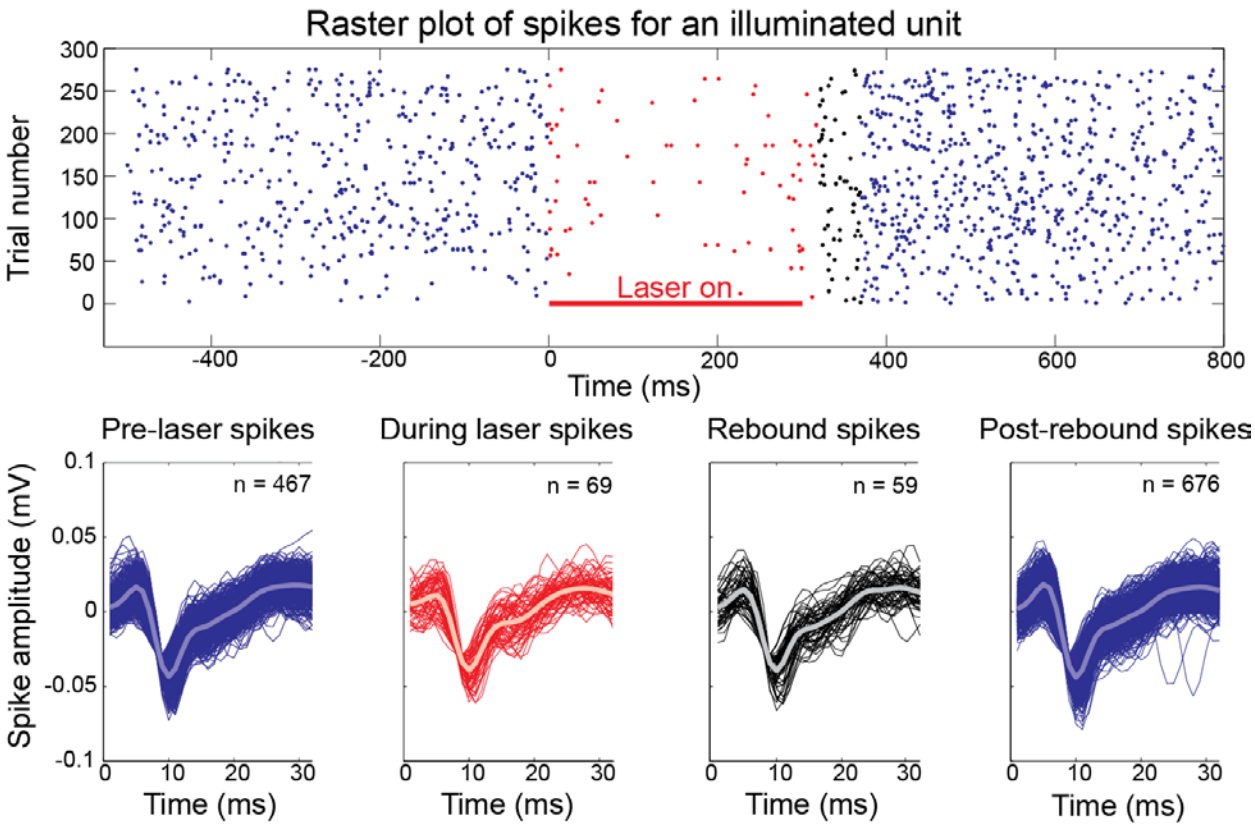

Supplementary Figure 14. Sample waveform.
The top panel shows the raster plot of all illuminated trials for a sample unit. Each dot represents a single spike. In the four panels below are the waveforms for each spike. From left to right, the panels represent pre-illumination spikes, spikes during illumination, spikes during the rebound, and spikes in the post-rebound period. The average spike waveform for each epoch is shown as the lighter colored overlay in the bottom panels. The waveform retains essentially the same shape throughout, though the amplitude is smaller for the spikes during illumination and immediately after during the rebound period.

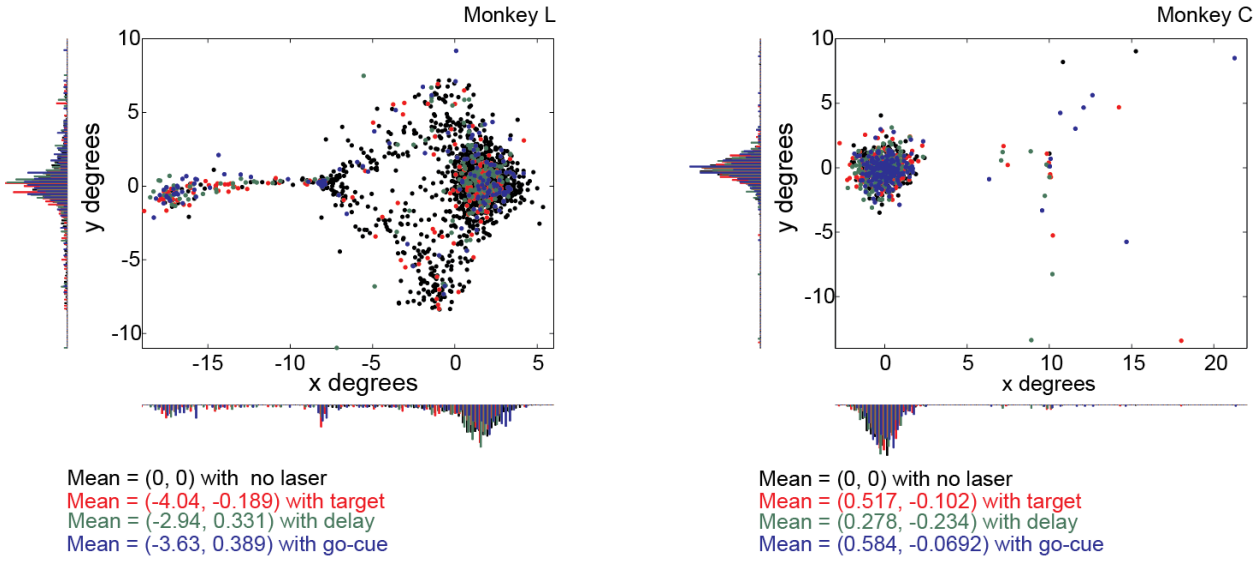

Supplementary Figure 15. Scatter plots of saccade end points

Saccade end points (normalized to the average of the no laser trial end points) for both monkeys for all trials in which a saccade was executed (correct, incorrect, and premature). While there is not a systematic deviation as was seen with optogenetic inactivation of the superior colliculus (Cavanaugh et al., 2012), saccades show a broader spread of endpoints in the laser trials than in the trials without illumination.

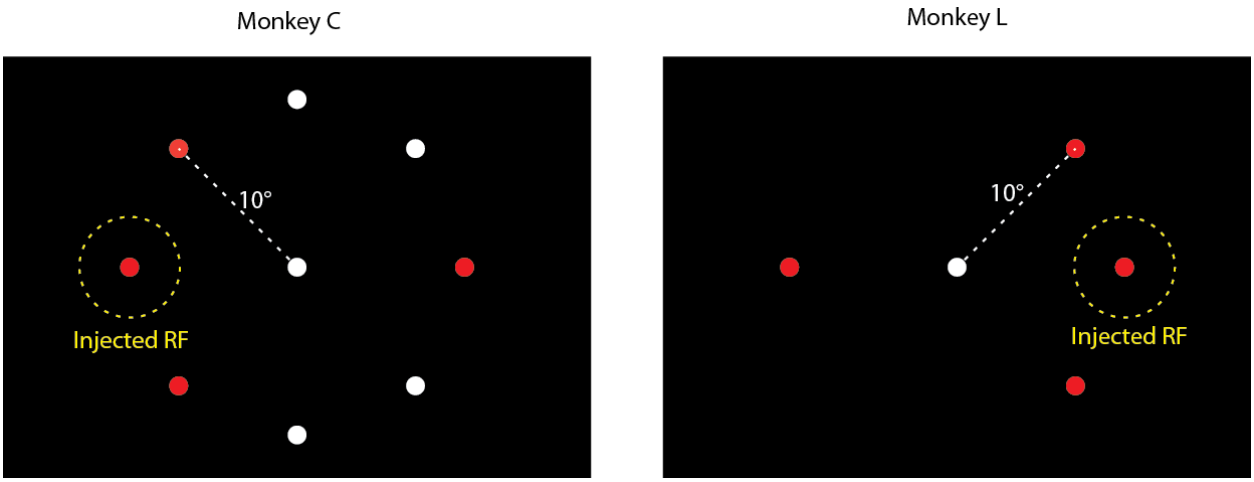

Supplementary Figure 16. Injection fields and target presentation locations for both monkeys
The receptive field corresponding to the center of the injection site is denoted by a dashed yellow circle. All possible target locations (10 degrees eccentric to center) are shown; however, only one target appeared per trial. The central fixation dot appeared on every trial. Both the target and the fixation dot were shown as white 1 degree diameter circles. In the diagram above, targets that were presented only with sham illumination are shown in white; those with both sham and laser illumination are shown in red. More targets were shown for monkey C than for monkey L due to differences in the animal's facility with the task. After the first day of inactivation, monkey L began to avoid targets on the injected side during testing (but not during calibration, implying a behavioral issue rather than physical damage). Consequently, only target locations in which we also illuminated were presented to monkey L subsequently. As shown above, this included the injected RF, the two adjacent target locations, and the target location 180 degrees opposite to the injected RF. Because the task was more difficult for monkey L at baseline, the error rates for targets on the side of the injected RF (which had 3 targets) were higher than those with for the contralateral side, which only had one target.

Supplementary Note

The light power density (mW /mm^2) on the surface of the ruby sphere as a function of fluence rate (photons / second) can be expressed as shown in Equation 1.

$$\Phi_{rs} = m*x / C \quad (1)$$

Where Φ_{rs} is light power density on the surface of the ruby sphere probe, x is fluence rate (photons / second) at the ruby wavelength(s), C is a constant correction factor determined to be 3.08 as shown below, and m is the probe- and wavelength-specific slope of the linear curve fit during the isometric probe calibration. Note that the y-intercept for that linear curve fit is set to 0.

The constant correction factor, C, is determined via Equation 2.

$$C = (1 + f_{H2O\text{-}cortex})* A_{cross\ section} / (A_{surface} *(1 - f_{blocked})) \quad (2)$$

Where $\boldsymbol{f_{H2O\text{-}cortex}}$ is the fraction by which calibration in water over estimates photon counts in cortex, $\mathbf{A_{cross\ section}}$ is the cross-sectional area of the ruby sphere (πr^2), the area over which collimated light is applied, $\mathbf{A_{surface}}$ is the surface area of the ruby sphere over which it (theoretically) can absorb photons ($4\pi r^2$), the area over which light is applied in vivo, and $\mathbf{f_{blocked}}$ is the fraction of the ruby sphere probe surface area that is blocked by the attached optical fiber and cannot absorb photons. $\mathbf{A_{cross\ section}}$, $\mathbf{A_{surface}}$, and $\mathbf{f_{blocked}}$ are all geometric properties of the isometric probe; however, the derivation of $\boldsymbol{f_{H2O\text{-}cortex}}$ is a bit more nuanced and, thus, explained below.

The difference in the refractive indices of water (n_{H2O} = 1.33) and the ruby (n_{ruby} = 1.77, provided by Edmund Optics) is slightly larger than the difference in the refractive indices of cortex (n_{cortex} = 1.37) (87) and the ruby. Thus, the critical angle in for the ruby in water is slightly smaller than the critical angle in cortex. The critical angle for total internal reflection of photons inside the ruby in both air and water was determined using **Equations 3** and **4.**

$$\Theta_{critical\_H2O} = arc(n_{H2O} / n_{ruby}) \quad (3)$$

$$\Theta_{critical\_cortex} = arc(n_{cortex} / n_{ruby}) \quad (4)$$

Snell's law was used to derive an expression for the angle of transmission, Θ_t, relative to the incident angle Θ_i (**Equations 5 and 6**).

$$\Theta_{t\_H2O} = \arcsin(n_{ruby} * \sin(\Theta_i) / n_{H2O}) \quad (5)$$

$$\Theta_{t\_cortex} = \arcsin(n_{ruby} * \sin(\Theta_i) / n_{cortex}) \quad (6)$$

Fresnel's Equations were rearranged to get reflection and transmission coefficients as a function of the incident angle for both the parallel and perpendicular cases as shown in **Equations 7 -10**. The terms parallel and perpendicular are relative to the plane of incidence.

$$\boldsymbol{R_{||}} = \frac{\boldsymbol{tan(\Theta i - \Theta t)}}{\boldsymbol{tan(\Theta i + \Theta t)}} \quad (7)$$

$$\boldsymbol{R_{\perp}} = \frac{\boldsymbol{sin(\Theta i - \Theta t)}}{\boldsymbol{sin(\Theta i + \Theta t)}} \quad (8)$$

$$\boldsymbol{T_{||}} = \frac{\boldsymbol{2*sin(\Theta t)*cos(\Theta i)}}{\boldsymbol{sin(\Theta i+\Theta t)*cos(\Theta i-\Theta t)}} \quad (9)$$

$$T_{\perp} = \frac{2*sin(\theta t)*cos(\theta i)}{sin(\theta i+\theta t)} \quad (10)$$

The percentages of light reflected and transmitted for a given incident angle were determined using the conservation of energy and then integrated over all possible incident angles to yield an overall percentage of photons emitted by the ruby sphere and then transmitted out of the ruby sphere back to the medium. In **Equation 11** below, the first term represents the fraction of fluoresced photons that are reflected back into the ruby sphere when emitted angles are less than the critical angle. The second term represents the angles over which 100% of photons remain in the ruby sphere.

$$\int_{\theta_i=0°}^{\theta_i=\theta_c} r(\theta_i)d\theta_i + \int_{\theta_i=\theta_c}^{\theta_i=90°} d\theta_i \quad (11)$$

These equations were solved empirically in MATLAB using $d\theta_i$ = 1°. It was determined empirically that water yields a photon count 3.8% higher than expected in cortex. This procedure was repeated for measurements and estimations in air v. water as well to confirm the correction. Theoretically, air should give a photon count 29.3% higher than expected in water and the measurements were 28.2 +/- 2.6% (standard error) higher in water than in air, which empirically confirms the validity of this theory-derived correction.

Supplementary Methods

Large-volume illuminator quality control. To ensure uniform light emission along the etched fiber tip, the illuminator was lowered with a micromanipulator (Siskiyou) into an integrating sphere (ThorLabs) in 500 µm increments through a diaphragm of custom shielding (light absorbing foil on the outside, aluminum foil facing inward) with a 26-gauge hole, sized such that no ambient light or light from parts of the fiber above the sphere could enter the integrating sphere. The total light power output was measured along the length of the illuminator and plotted as a function of how far the illuminator had been lowered into the integrating sphere. To confirm that the large-volume illuminator does not lose light energy due to its geometry, light power measurements from a flat cleaved optical fiber and the illuminator were compared under identical input conditions. After initial tests showed identical total light power output for the current illuminator and flat-cleaved fibers, this testing was not continued.

Isometric light probe construction. A 300 µm diameter spherical ruby ball lens (Edmund Optics) was centrally affixed to the flat-cleaved, polished end of a 400 µm diameter multimode optical fiber (ThorLabs, NA = 0.48) with optically-transparent, UV curable adhesive (NT37-322, Edmund Optics). An SMA connector was fixed to the other end of fiber (SMA904, ThorLabs). The isometric light probe (**Fig. S2**) was then coupled to a CCD spectrometer (Ocean Optics) via the SMA connection. After subtracting out a dark spectrum and correcting for non-linearity, light probe fluorescence was measured with the CCD spectrometer and recorded with SpectraSuite software (Ocean Optics) running on a PC. All recorded spectra were saved in their raw form without averaging. To prevent saturation near the ruby wavelength (690 - 695 nm), the spectrometer integration duration was adjusted in the range of 3 ms to

3 s, with most integration times in the 0.1 to 1 s range. Only the ruby peak was used in analysis. All photon counts were converted to fluence rates with units of photons/second offline.

Isometric probe calibration. The linear relationship between incident light power density at the test wavelength and induced ruby fluorescence was determined for each probe (**Fig. S4**). A beam of collimated light was generated by coupling a DPSS (532 nm and 635 nm, SLOC) or diode (473 nm, Vortran) laser to a large-diameter collimator (ThorLabs) via a 200µm diameter (NA = 0.22) multimode FC/PC terminated fiber (ThorLabs). The collimator was fixed in an externally threaded optic mount adapter (SM1P1, Thor Labs), and the external threading was screwed into a custom iris made of light-absorbing, black ABS plastic and coated with a light absorbing paint (Krylon). The custom iris was mounted and aligned to focus the beam centrally on a beam profiler (ThorLabs) that had been calibrated for absolute light power measurements. After collecting the total light power and beam uniformity measurements, a beam of collimated light, at light power densities of 0.5 to 4.5 mW / mm^2 in 0.25 mW / mm^2 increments, was applied to the light probe in water via a custom-built water bath. A linear relationship was determined between incident light power density and the emitted ruby photon count. The emitted ruby photon count was defined as the sum of all photons in the 0.47 nm-wide bin with peak amplitude between 693 nm and 697 nm. The slope was corrected to account for the slight difference in the refractive indexes of the brain (n = 1.37) and water (n = 1.33) and for the difference in the angle between the light source and probe during calibration (90°) and testing (72°). Each calibration was performed with exactly the same probe and light color as was used in testing. The probe was initially connected to the spectrometer for calibration and the connection was maintained until the end of testing with that probe.

Planar illuminator. A flat-cleaved and polished 1.5 mm diameter (NA = 0.5) plastic optical fiber (Industrial Fiber Optics) was affixed centrally in a custom, 3D printed aligner. For red (635 nm) and green (532 nm) light tests, an analog, fiber-coupled DPSS laser was connected to a TTL-controlled optical shutter (OzOptics) via a 200 µm diameter (NA = 0.22) multimode FC/PC terminated fiber. For 473 nm light, a fiber-coupled diode laser (Vortran) was used. The output from the shutter was FC coupled to the planar illuminator. The light power output from the planar illuminator was measured prior to each testing session by lowering it into an integrating sphere (ThorLabs) with attached power meter (ThorLabs) in 0.25 mm steps. The planar illuminator was used to approximate a wide collimated-beam source because using an actual wide collimated beam source was not physically possible in the *in vivo* preparation. In order to get a collimator with uniform light power output over a 1.5 mm diameter area, the collimator itself would need to be much larger than the mouse's head and only the very center of the collimated beam would be uniform enough for testing. While we initially attempted to use the iris with a very small aperture and large physical footprint that was used for calibration for the in vivo prep, we found it was not practical. Thus, we used a planar illuminator. Instead we profiled the beam of the planar illuminator and found it to be of uniform output (+/- 10%) over a centrally located 1 mm^2 area in the center of the beam even at a distance 8 mm away.

Monte Carlo Modeling. Monte Carlo modeling was performed in MATLAB using the Henyey-Greenstein anisotropic scattering model, 1e6 photons launched per voxel, and voxel size 50µm x 50µm x 50µm, as described previously.[28] Absorption and scattering coefficients of 2.14 cm^{-1} and 6.61 cm^{-1}, respectively, were used, as determined for 635 nm light. All illuminators had NA=0.5, as this is a property of the

optical fiber used (Industrial Fiber Optics, Inc.) NA =0.5 yields a half opening angle of 30 degrees. The novel illuminator was modeled as two 3mm long sheets of light angled as per the tip with a 30 degree downward bias, as per the NA. In a 3D model, these lines of light would be rotated in all direction, but in **Fig. S9** we only show the middle voxel, as its diameter (50 µm), corresponding to the diameter of a large neuron. Light exiting out the base of the new illuminator is ignored for simplicity and based on calibration data demonstrating that at least 90% of light, and typically more, exits out the sides, not the tip. The conventional optical fiber is shown at the middle voxel with equal light power density to the novel illuminator in **Fig. S9**. The planar illuminator was modeled at its diameter of 1.5mm with NA=0.5. In **Fig S7**, the middle 6 voxels of the planar illuminator model were summed to yield the light distribution over the 300 µm diameter of the isometric light probe.